Journal of Solid State Chemistry 184 (2011) 747–752

Contents lists available at ScienceDirect

Journal of Solid State Chemistry

journal homepage: www.elsevier.com/locate/jssc

Ag adsorption on Cd-terminated CdS (0 0 0 1) and S-terminated CdS (0 0 0 $\bar{1}$) surfaces: First-principles investigations

Yandong Ma, Ying Dai*, Wei Wei, Xianghong Liu, Baibiao Huang

School of Physics, State Key Laboratory of Crystal Materials, Shandong University, Jinan 250100, People's Republic of China

ARTICLE INFO

Article history:
Received 28 November 2010
Received in revised form
26 January 2011
Accepted 31 January 2011
Available online 4 February 2011

Keywords:
DFT
Adsorption
Ag@CdS
Interface
Surface

ABSTRACT

First-principles calculations are performed to study the adsorption of Ag at Cd-terminated CdS (0 0 0 1) and S-terminated CdS (0 0 0 $\bar{1}$) surfaces as a function of Ag coverage. Our results reveal that Ag adsorption at Cd-terminated (0 0 0 1) has a large binging energy than at S-terminated (0 0 0 $\bar{1}$) surface. For Ag adsorption at Cd-terminated (0 0 0 1) surface, *T*4 structure is more favorable and the Ag–Cd bond posses an ionic-like character. While for Ag adsorption at S-terminated (0 0 0 $\bar{1}$) surface, the *H*3 structure is most stable and the bonding between Ag–S is covalent. It is found that the magnitude and the sign of surface dipole moment are partly determined by the difference between the electronegativities of Ag and the host atom bonding with Ag. The adsorption energy changes as a function of Ag coverage. In addition, related properties of Ag cluster adsorption at Cd-terminated (0 0 0 1) surface are also discussed.

1. Introduction

Hybrid metal@semiconductor nanoparticles have recently attracted considerable interest due to their prospective technological importance in the field of optical, catalysis and electronics [1–6]. This interest stems from the possibility of exploiting the combination of properties from the semiconductor (electrical or optical) and from the metal (optical, electrical, chemical, and connectivity) [7]. Ag is usually a promising candidate to modify semiconductor materials due to its high exchange-current density, low activation energy and inexpensiveness. In fact, silver@semiconductor composite systems, such as Ag@$BiVO_4$ [8], Ag@TiO_2 [9,10], Ag@AgCl [11–14], Ag@AgBr [15,16], have been investigated, and it has been identified that these systems performed outstanding properties compared with corresponding bare semiconductors. In these systems, Ag can improve charge separation and promote charge–transfer process at the silver@semiconductor interface. Recently, intense research activity devoted to hybrid nanoparticles is especially focused on Ag@CdS composite [17–21]. Gong et al. [17] investigated the optical properties of synthesized chitosan Ag@CdS core shell composite, which exhibited a large third-order nonlinear response. The effective nonlinear absorption coefficient of Ag@CdS composite was found to be 400 times larger than that of bare CdS. Kumar and Chaudhary [18] studied photophysical properties of Ag@CdS composite synthesized by simple mixing of two colloidal solutions prepared separately or by adding Ag nanoparticles to a Cd^{2+} solution prior to the precipitation of CdS. In this study, it revealed that a charge–transfer complex was formed between CdS and Ag, in which the degree of electron transfer was controlled by the amount of Ag. Moreover, they have studied the emission properties of Ag-adenine-templated CdS nanohybrids [19]. Priya et al. [20] observed an enhancement in luminescence of CdS particles at low silver content in Ag@CdS composite synthesized by a colloidal method, which was attributed to an increased local field by silver surface plasmons. While, at high silver concentration during the aging process, the formation of silver clusters was increased, and luminescence quenching was observed due to the resonance electron transfer to metallic surfaces. Simerjeet and Louisa [21] synthesized monolithic mesoporous aerogels comprising CdS partially coated with metallic Ag, and it was shown that the concentration of Ag had a significant impact on the resultant Ag@CdS aerogel morphology and the change in optical response. They showed that the increase in photoluminescenece intensity of CdS was attributed to the formation of a relatively long-lived charge–transfer complex between excited CdS and Ag.

Wurtzite CdS is an *n*-type semiconductor. The conduction band of wurtzite CdS is around −1.0 V vs NHE [18], and the Fermi level of Ag is at +0.15 V [22]. This large potential difference between the conduction band of CdS and the Fermi level of Ag leads to the formation of a Schottky barrier. The electron migration from CdS to Ag occurs until the two levels are aligned since Ag has a work function higher than that of CdS. As a result, the surface of Ag exhibits an excess negative charge, while CdS acquires an excess positive charge. The Schottky barrier forms

* Corresponding author.
E-mail address: daiy60@sdu.edu.cn (Y. Dai).

0022-4596/$ - see front matter © 2011 Elsevier Inc. All rights reserved.
doi:10.1016/j.jssc.2011.01.043

at the interface of Ag@CdS composite. The barrier height is defined as the difference between the CdS conduction band and the Fermi level of Ag. Therefore, a Schottky barrier formed at Ag and CdS interface can serve as an efficient electron trap to avoid the electron–hole recombination, which is responsible for the excellent performance of Ag@CdS system observed in experiments.

Despite progress in these experimental studies, an understanding of the fundamental mechanisms of Ag@CdS composite is still in its infancy. In particularly, the contact property of Ag at CdS surface is not well comprehended. An understanding of this is important for obtaining a deeper insight into the relevant mechanisms on atomic scale and improving growth in controlled fashion [23,24]. *Ab initio* calculations are useful complement to experimental studies for Ag@CdS interface. Consequently, it is of fundamental interest in obtaining insight into the absorption properties of Ag at CdS surface. To the best of our knowledge, there have been no theoretical studies reported on the absorption properties of Ag at CdS surface. In this paper, we examine the geometric and electronic properties of Ag at Cd-terminated wurtzite CdS (0 0 0 1) and S-terminated (0 0 0 $\bar{1}$) surfaces, which are the two most common surfaces of CdS, by means of first-principles calculations, and speculate work function, ionization potential, and electron affinity of clean and Ag adsorbed Cd-terminated (0 0 0 1) and S-terminated (0 0 0 $\bar{1}$) surfaces to understand its physical properties. Moreover, the adsorption of small Ag cluster (Ag_2, Ag_4 and Ag_7) at Cd-terminated (0 0 0 1) surface is also investigated in order to elucidate Ag atoms' aggregation and nucleation properties.

2. Computational methods

The total-energy density functional theory (DFT) calculations have been performed within the generalized gradient approximation (GGA) for the exchange-correlation effects via Perdew–Burke–Ernzerhof (PBE) functional [25], using plane-wave basis sets and projector augmented waves (PAW) method [26,27] as implemented in the Vienna *ab initio* Simulation Package (VASP) [28]. The energy cutoff for the basis function is 400 eV. A $4\times4\times1$ Monkhorst–Pack mesh [29] is used for the Brillouin zone integration. Both Cd-terminated CdS (0 0 0 1) and S-terminated CdS (0 0 0 $\bar{1}$) surfaces are simulated using a slab model of 2×2 surface unit cell periodicity consisting of eight CdS bilayers, of which the lowest four bilayers are fixed in the optimized bulk configuration (as shown in Fig. 1). The upper four bilayers and any adatoms or clusters are allowed to fully relax until all atomic forces are smaller than 0.02 eV/Å. Relaxation in the forth bilayer is negligible indicating that a sufficiently large slab is employed. The vacuum thickness between two neighbor slabs is 20 Å. Because it indicates qualitatively credible results with respect to silver adsorption on the Cd-terminated (0 0 0 1) and S-terminated (0 0 0 $\bar{1}$) surfaces based on the adopted 2×2 surface unit cell, we would not discuss the effects of the surface reconstruction on the adsorption properties in the present work.

To approximate these slab calculations to a single calculation, and as such to correctly relax only one single facet to its lowest energy configuration, we have prevented the bottom dangling bonds by passivating of the bottom layers with pseudohydrogen atoms to remove undesirable surface states and the interaction between surfaces and thus to reduce the computational cost by decreasing the number layers. For each Cd–S bond in the wurtzite CdS, the Cd and S atoms contribute 0.5 and 1.5 e^-, respectively. Therefore, for Cd-terminated (0 0 0 1) surface (termed as CS), the 1.5 e^- fraction charges associated with dangling bonds in the S bottom layer are saturated with pseudohydrogen atoms, each

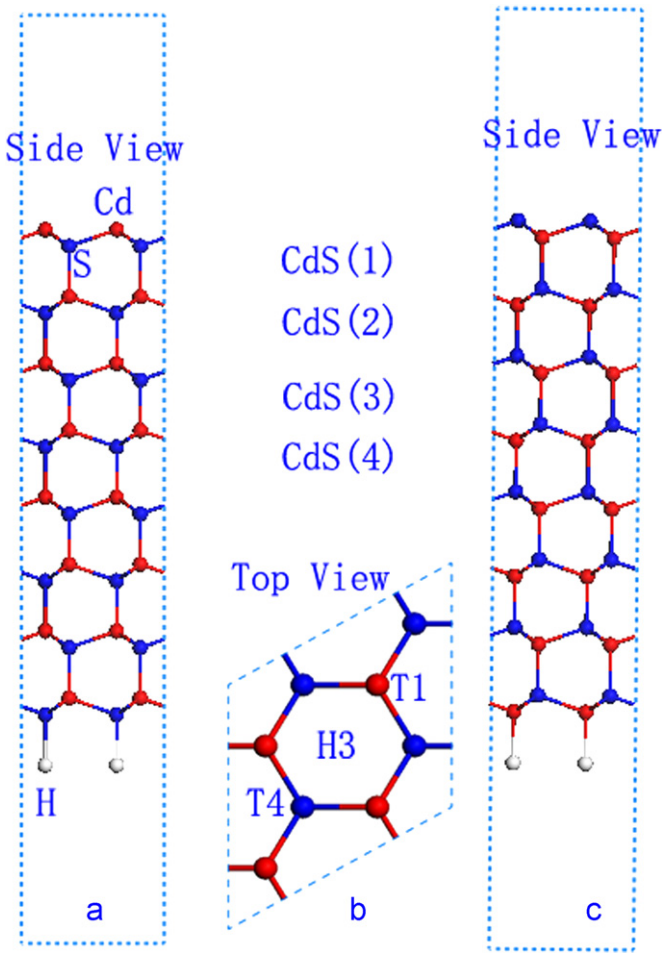

Fig. 1. Side views of the relaxed atom configurations of (a) CS, and (c) SS; (b) top view of the relaxed CS and SS. *H*3 is the hollow site, *T*1 is the site directly above the S atom of the CdS(1) bilayer, and *T*4 is the site directly above the Cd atom of the CdS(1) bilayer. The gray, red, and blue spheres represent H, Cd, and S atoms, respectively. (For interpretation of the references to color in this figure legend, the reader is referred to the web version of this article.)

with a fractional charge of 0.5 e^-. While for the S-terminated (0 0 0 $\bar{1}$) surface (termed as SS), the 0.5 e^- fraction charges associated with dangling bonds in the Cd bottom layer are saturated with pseudohydrogen atoms, each with a fractional charge of 1.5 e^-. This dangling bond saturation is a standard computational artifact to ensure unphysical charge transfer between the two ends of the slab and avoid the appearance of spurious surface states in the gap of the semiconductor [7,30–32]. This computational artifact is based on the fact that even when bottom surface is passivated with pseudohydrogens, the band structure (except surface states) is similar to the bulk band structure [33]. Namely, for CS (SS), and the Cd (S) surface states at the Fermi level (E_F) remain exactly the same when the bottom S (Cd) surface states are moved away from E_F due to the passivation. The calculated lattice constants of wurtzite bulk CdS are $a=4.18$ Å, $c=6.81$ Å and the Cd–S bond length is 2.56 Å. All these constants are in good agreement with the former experimental and theoretical studies [32,34–36]. Total energy calculations for an Ag atom and Ag clusters are performed within a cubic box of side length 15 Å. The silver adsorption induced dipole moment is taken into account using a dipole correction in our calculations [37].

In this work, the energy required for the adsorption of Ag atoms or Ag clusters (Ag_2, Ag_4 and Ag_7) on the CS and SS is

calculated by

$$E_{ad} = \frac{1}{N}(E_{total} - E_{ref} - NE_{adsorbate}),$$

where E_{total} and E_{ref} are the total energy of the covered surface and the corresponding clean surface, respectively, $E_{adsorbate}$ is the energy of Ag adsorbate in the gas-phase and N is the number of adsorbates (Ag atoms or cluster).

3. Results and discussion

3.1. Work functions, ionization potential, and electron affinity of clean CS and SS

To examine the Ag adsorption properties, we first elucidate the related properties for clean CS and SS, i.e., work function (*WF*), ionization potential (*IP*), and electron affinity (*EA*) (as shown in Fig. 2). The *IP* is defined as the energy difference between vacuum level (E_{vac}) just outside the surface and valence band maximum (E_{VBM}) deep inside the solid, which depends on the surface dipole and thus surface orientation. The vacuum level is determined from the self-consistent, plane-averaged potential (V_{av}), in the middle of the slabs along the direction perpendicular to the surfaces. It can be obtained from the Poisson's equation [38],

$$\frac{\partial^2}{\partial z^2} V_{av}(z) = -4\pi\rho_{av}(z),$$

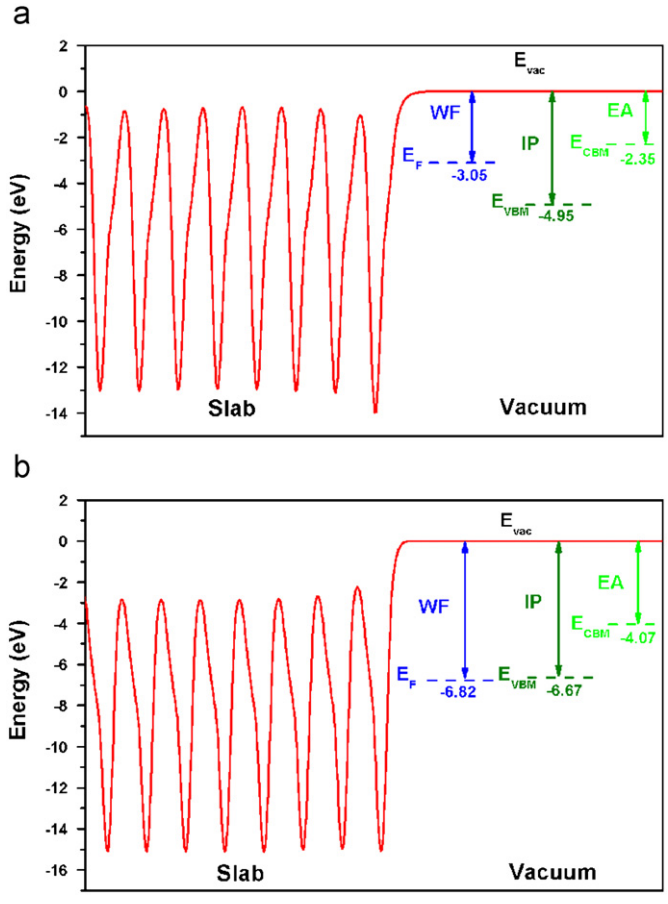

Fig. 2. Planar average of the electrostatic potential (red) for the relaxed: (a) CS and (b) SS. E_{VBM}, E_{CBM}, E_{vac}, and E_F represent the top of the valence band, the bottom of the conduction band, vacuum level, and the Fermi level, respectively. (For interpretation of the references to color in this figure legend, the reader is referred to the web version of this article.)

and is given by the relation

$$V_{av}(z) = -4\pi \int_z^{\infty} \rho_{av}(z')z'dz' + 4\pi z \int_z^{\infty} \rho_{av}(z')dz',$$

in which

$$\rho_{av}(z) = \frac{1}{A}\iint_A \varphi^2(x,y,z)dxdy$$

WF is the difference between the vacuum level and the Fermi energy (E_F). *EA* is calculated as the energy difference between the vacuum level and the bottom of conduction band (E_{CBM}): $\chi = E_{vac} - E_{CBM}$. However, we confront with the well-known underestimation of band gap in DFT calculations related to the inability of DFT to describe properly the unoccupied states. In order to overcome this shortcoming, we add the experimental band gap to the calculated valence band maximum to get the conduction band minimum, as introduced in former theoretical studies [39–42]. Fig. 2 displays the plane-averaged potentials for CS and SS. For CS, the *WF*, *IP* and *EA* are 3.06, 4.92 and 2.32 eV, respectively, while these values are 6.82, 6.60 and 4.00 eV for SS. All these results are shown in Table 1.

3.2. Geometric and electronic structure

To examine the adsorption properties, we consider a single Ag atom adsorbed at both CS and SS, which corresponds to the coverage of 0.25 monolayer (ML). As shown in Fig. 1b, we consider three possible adsorbed structures *T*1, *T*4 and *H*3 for both CS and SS. All the initial arrangements of the three structures are fully relaxed. For Ag at CS, the *T*4 structure is most stable, in which the bond length d_{Cd-Ag} is about 2.63 Å and the adsorption energy is about −2.47 eV. While for Ag at SS, the *H*3 structure is more favorable, in which the averaged Ag–S bond length d_{S-Ag} is 2.55 Å and the adsorption energy is −3.68 eV. Such large negative adsorption energies suggest that the reaction between Ag and CdS is strongly exothermic, especially on SS.

Fig. 3 plots the total density of states (TDOS) of adsorbed Ag and each CdS bilayer for relaxed CS and SS. The labels in Fig. 3 for bilayers are the same as in Fig. 1. It can be seen that the electronic states of CdS bilayers near the surface are different from those deep inside the solid. The Ag-induced changes in electronic structures mainly concentrate on surface region and decay quickly with the increase of site depth from surface. For CS (Fig. 3a), the TDOS of the forth plane below surface already resembles closely that of the bulk. While for the TDOS of SS (Fig. 3b), only small perturbations caused by Ag at the third plane below surface are visible. These results indicate that significant relaxation is limited to the top three bilayers for the adsorption of

Table 1
Calculated structure parameters for Ag adsorption at CS and SS with different coverage Θ. E_{ad} is the energy for the adsorption of Ag atoms. d is the optimized bond length between Ag and the nearest host atom. Φ is the work function, $\Delta\Phi$ is the change of work function with respect to clean surface. μ is the surface dipole moment.

Θ	E_{ad} (eV)	d (Å)	Φ (eV)	$\Delta\Phi$ (eV)	μ (Debye)
CS					
0.25	−2.47	2.631	3.07	0.01	0.02
0.5	−2.21	2.631	4.24	1.18	1.10
0.75	−2.07	2.728	4.18	1.12	0.69
1.00	−1.69	2.750	4.20	1.14	0.53
SS					
0.25	−3.72	2.546	5.92	−0.89	−1.65
0.50	−3.37	2.583	5.03	−1.79	−1.66
0.75	−2.70	2.589	3.20	−3.61	−2.24
1.00	−2.31	2.588	3.19	−3.62	−1.68

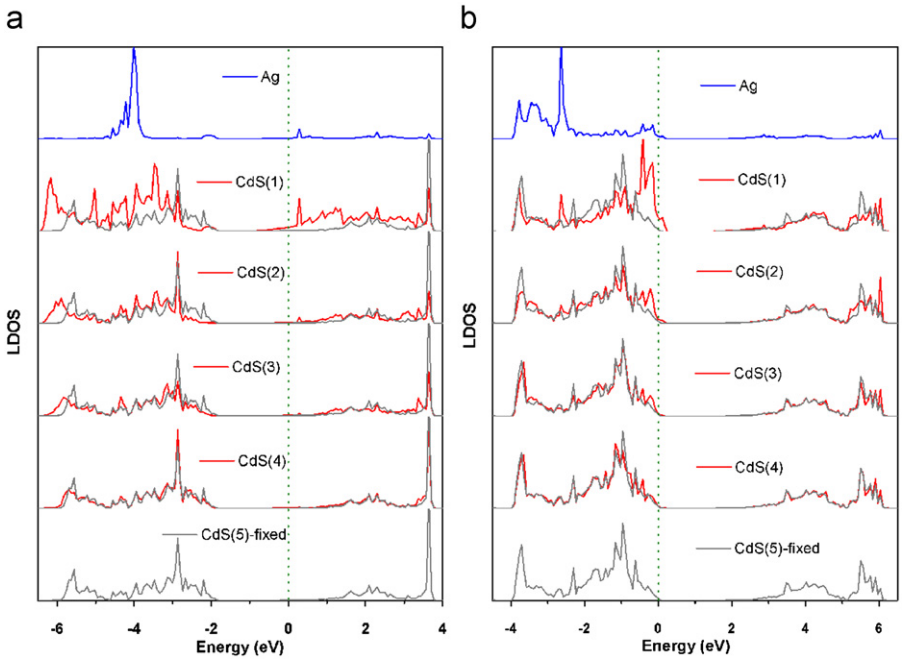

Fig. 3. TDOS for adsorbed Ag and each CdS bilayers from relaxed: (a) CS and (b) SS. The labels for bilayers are the same as in Fig. 1. The TDOS of the relaxed bilayers (CdS(1)–CdS(4)) (red lines) contain the TDOS the of the fixed CdS(5) bilayer (gray lines) for comparison. The dotted lines represent the Fermi level. (For interpretation of the references to color in this figure legend, the reader is referred to the web version of this article.)

Ag at CdS surface, which also indicates that our models with eight bilayers are sufficient for examining the adsorption properties. At the interface, clear evidence of strong hybridization can be seen between the TDOS of Ag and CdS(1) bilayer for both CS and SS. To get a more detailed description about the interaction between Ag adatom and CdS surfaces, the projected density of states (PDOS) are calculated. For Ag adsorption at CS, the PDOS of Ag 4*d*/5*s*, and 4*d*/5*s* of Cd bonding to Ag are shown in Fig. 4a. It can be seen that the 4*d* states of both Ag and Cd are dominantly localized deeply inside the valence band. The overlapping between the localized Ag 5*s* and localized Cd 5*s* states indicates some ionic-like component of the Ag–Cd bond. The Fermi level lies in the bottom of the conduction band and the localized Ag 5*s* states just lie above the Fermi level. Therefore, excited electrons from CdS surface would occupy the Ag 5*s* states when this Ag@CdS system is activated. As a result, an acceptor is accreted, thus Ag adatom is assumed to play a mediating role in storing and shutting the photo-generated electrons from CdS to acceptor in a photocatalytic process for this Ag@CdS system. This would be responsible for the high photocatalytic activity of Ag@CdS system observed in experiments. For an Ag atom adsorption at SS, the PDOS of Ag 4*d*/5*s* and 3*p* states of S atom bonding to Ag atom plotted in Fig. 4b shows that the delocalized S 3*p* states are divided into two main regions, which indicates the formation of bonding and antibonding states. Different from that of Ag adsorption at CS, Ag 4*d* states are more delocalized and hybridized with S 3*p* states, which reveals that the Ag–S bonding is covalent. It should be mentioned that the photocatalytic activity is a complex property which is related with many factors. Our DOS can only give the interaction information between Ag and CdS surfaces. From Fig. 4, we cannot give the conclusion that which configuration has higher photocatalytic activity or whether the two configurations have the same photocatalytic activity.

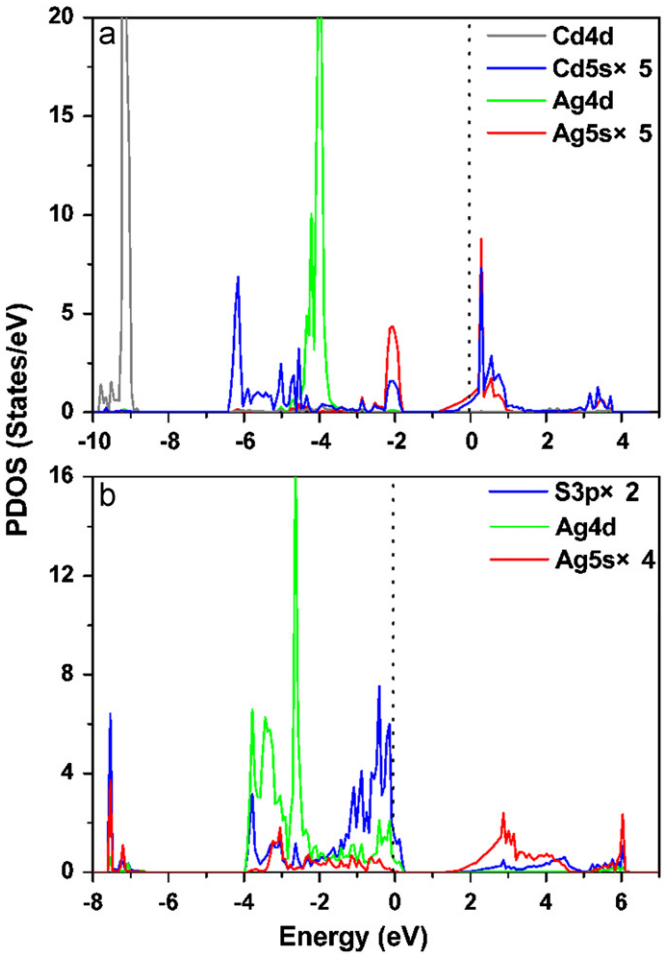

Fig. 4. Projective density of states (PDOS) for single Ag atom adsorption on the (a) CS and (b) SS. The dotted lines represent the Fermi level.

3.3. *Work function change and surface dipole moment*

The magnitude and the sign of work function change ($\Delta\Phi$) can be used to determine the direction and extent of electron

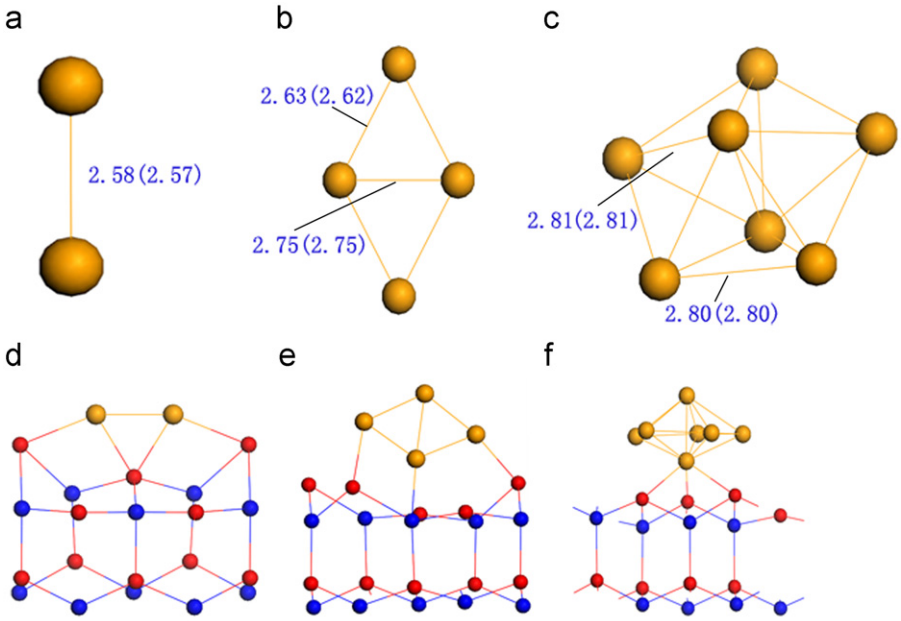

Fig. 5. Calculated ground state geometries of: (a) Ag_2, (b) Ag_4, and (c) Ag_7. The bond lengths are in Å. For comparison, bond lengths obtained in Ref. [45] are shown in parentheses. Energetically favored adsorption configurations for Ag_2, Ag_4, and Ag_7 on CS surface are shown in (d), (e), and (f), respectively. Only the two top bilayers of CdS surfaces are shown. The orange, red, and blue spheres represent Ag, Cd, and S atoms respectively. (For interpretation of the references to color in this figure legend, the reader is referred to the web version of this article.)

redistribution. Table 1 shows the $\Delta\Phi$ induced by Ag adsorption for both surfaces. It can be seen that work function changes for both surfaces due to the surface dipole moments arising due to a significant electron transfer between the substrate and the adatom. Namely, $\Delta\Phi$=0.01 eV for Ag adsorption at CS and $\Delta\Phi$= −0.89 eV for Ag adsorption at SS. The work function changes can be expected partly due to the large difference of electronegativity between host atom and Ag atom. The Pauling electronegativities are 2.58, 1.69, and 1.93 for S, Cd, and Ag atoms, respectively, thus a positive $\Delta\Phi$ is expected on the CS, while a negative $\Delta\Phi$ is expected on SS. In addition, the difference of electronegativities between S and Ag atom is significantly larger than that between Cd and Ag atom. Therefore, compared with Ag adsorption at CS, a larger absolute value of $\Delta\Phi$ induced by Ag adsorption can be expected for Ag adsorption at SS.

Using the Helmholtz equation, the surface dipole moment (in Debye) can be evaluated by [43]

$$\mu = (1/12\pi)A\Delta\Phi/\Theta,$$

where A is the area in Å^2 per (1×1) surface unit cell, $\Delta\Phi$ is the work function change in eV, and Θ is the coverage. Then the surface dipole moments are μ=0.02 and −1.65 Debye for Ag adsorption at CS and SS, respectively. The dipole moment can be viewed as being proportional to the product of the effective charge on Ag atom and the vertical distance between Ag and host atom bonding to Ag. With the understanding that the optimized vertical Ag–Cd distance is larger than that of Ag–S, we can obtain that a larger value of the effective charge on the Ag adatom can be expected on SS than that on CS. Namely, the charge redistribution between the Ag and SS is more significant than that between Ag and CS, which is in agreement with the above discussion. Despite the overall charge transfer, the detailed charge redistributions are site dependent, which determines the magnitude and the sign of $\Delta\Phi$ as well as the surface dipole moment [44]. Moreover, the small absolute value of the dipole moment of Ag adsorption at CS is affected by specific atomic geometry.

3.4. Coverage-dependent surface properties

In order to understand better the interface properties, calculations are performed for Θ=0.50, 0.75, and 1.00 ML of silver coverage, which correspond to two, three, and four Ag atoms adsorption on the 2×2 surface unit cell. The calculated adsorption energies E_{ad}, bond lengths between Ag and nearest host atom d, work function changes $\Delta\Phi$, and surface dipole moments μ are summarized in Table 1. It can be seen that, for CS, the adsorption energies per Ag atom become larger with silver coverage increase (i.e., from −2.47 eV for 0.25 ML to −1.69 eV for 1.00 ML), indicating strong repulsive interaction between the Ag adatoms. Therefore, with appropriate Ag chemical potential, the adsorption of Ag at CS could favor lower coverage situation. This is also confirmed by the increased bond lengths d_{Ag-Cd} with coverage increase. This coverage dependent behavior is also found for Ag adsorption at SS, but the absolute value of the adsorption energy is much larger indicating that Ag atoms adsorption on SS is easier than on CS. In addition, for Ag adsorption at SS, the variation of adsorption energies with the increase of coverage is larger than that for CS indicating a relatively stronger repulsion between Ag adatoms. From Table 1, it can be seen that the work function decreases with the increase of coverage for Ag adsorption at SS, and a saturation value is reached when the coverage $\Theta > 0.75$ ML. For Ag adsorption at CS, work function increases rapidly when the coverage $\Theta < 0.5$ ML, while the work function changes little when the coverage $\Theta > 0.5$ ML, indicating a saturation value is also reached. This is due to that, at low coverage stages of Ag adsorption, with the coverage increase, the modification of overall charge redistribution between CdS and Ag would becomes strong, resulting in the absolute value of work function change increasing with Ag coverage. However, when the coverage is high enough, the surface dipoles on the surface interact with each other significantly, which leads to that the variation of work function change is neglectable with the increase of coverage. Thus, the work function change reaches a saturation value.

3.5. Ag clusters adsorption on CS

In order to investigate the Ag atoms' aggregation and nucleation, we further take CS as an example to consider the adsorption properties of Ag clusters on CS. Ag particles on the surface with different size should present different chemical and physical properties. Therefore, we consider three kinds of Ag clusters, i.e., an one-dimensional (1D) Ag_2 cluster, a two-dimensional (2D) Ag_4 cluster, and a three-dimensional (3D) Ag_7 cluster. The ground state structures of Ag_n ($n=2$, 4, and 7) employed in this study are those obtained in Refs. [45,46], as shown in Fig. 5a–c, respectively. The energetically favorable adsorption configurations are shown in Fig. 5d–f, respectively. For Ag_2, Ag_4, and Ag_7 on the CS, the calculated adsorption energies are -2.80, -4.05 and -4.59 eV, respectively. It can be noticed that adsorption energies of Ag cluster are obviously lower than that of a single Ag atom adsorption. In addition, the adsorption energies decrease with the increase of cluster size indicating that the adsorption of Ag atoms on CdS surface would attract more Ag atoms to cluster together and thereby form atomic islands.

It should be noted that, ideally, as CdS is an *n*-type semiconductor, this suggests that some S vacancies or/and Cd interstices may exist. Indeed, these intrinsic defaults deed to be at the origin of the *n*-type of the material. And such defaults are supposed to influence a lot the electronic structure and, in particular, the position of the Fermi surface. However, a fully investigation on these cases, clearly, is a very complex work. And our present work is limited within the scope of the CdS without intrinsic defaults. Further investigation is expected to be carried out to obtain a deeper insight.

4. Conclusions

The first-principles calculations are performed to investigate the geometric and electronic properties of Ag adsorption at CS and SS. Our results show that the adsorption of Ag on SS is more favorable than that at CS. The *H*3 structure is most stable for Ag adsorption at SS, while *T*4 structure is more favorable for Ag adsorption at CS. For single Ag adsorption at CS, the overlapping between the localized Ag 5*s* and localized Cd 5*s* states indicates some ionic-like component of Ag–Cd bond. While for single Ag adsorption on SS, Ag 4*d* states are more delocalized and hybridized with S 3*p* states revealing that Ag–S bonding is covalent. The results indicate the electronegativity difference between Ag and host atom bonding to Ag plays an important role for the magnitude and the sign of surface dipole moment as well as the change of work function. Our results indicate there is repulsive interaction between Ag adatoms on both CS and SS with the silver coverage increase. For Ag adsorbed at SS, the work function decreases with the increase of Ag coverage, and reaches saturation when the coverage $\Theta > 0.75$ ML due to the dipole–dipole interaction. For Ag adsorbed at CS, work function exhibits rapidly raising when the coverage $\Theta < 0.5$ ML, while the work function changes little when the coverage $\Theta > 0.5$ ML indicating a saturation value is also reached. For small Ag clusters (Ag_2, Ag_4, and Ag_7) adsorbed CS surface, adsorption energies are obviously lower than that of a single Ag adsorption, and the cluster adsorption energy decreases with the cluster size increasing, which indicates that the adsorption of Ag atoms on the CdS surface would attract more Ag atoms to cluster together and thereby form atomic islands.

Acknowledgments

This work is supported by the National Natural Science foundation of China under Grant 10774091 and 20973102, National Basic Research Program of China (973 Program, Grant 2007CB613302).

References

[1] G. Dukovic, M.G. Merkle, J.H. Nelson, S.M. Hughes, A.P. Alivisatos, Adv. Mater 20 (2008) 4306.
[2] E. Elmalem, A.E. Saunders, R. Costi, A. Salant, U. Banin, Adv. Mater 20 (2008) 4312.
[3] N. Bao, L. Shen, T. Takata, K. Domen, Chem. Mater 20 (2008) 110.
[4] V. Subramanian, E.E. Wolf, P.V. Kamat, J. Am. Chem. Soc. 126 (2004) 4943.
[5] R. Konta, T. Ishii, H. Kato, A. Kudo, J. Phys. Chem. B 108 (2004) 8992.
[6] K. Maeda, K. Domen, J. Phys. Chem. C 111 (2007) 7851.
[7] R. de Paiva, R. Di Felice, ACS Nano 2 (2008) 2225.
[8] S. Kohtani, J. Hiro, N. Yamamoto, A. Kudo, K. Tokumura, R. Nakagaki, Catal. Commun. 6 (2005) 185.
[9] A. Wold, Chem. Mater. 5 (1993) 280.
[10] Z.C. Shan, J.J. Wu, F.F. Xu, F.Q. Huang, H.M. Ding, J. Phys. Chem. C 112 (39) (2008) 15423.
[11] D. Schurch, A. Currao, S. Sarkar, G. Hodes, G. Calzaferri, J. Phys. Chem. B 106 (2002) 12764.
[12] S. Glaus, G. Calzaferri, R. Hoffmann, Chem. Eur. J. 8 (2002) 1785.
[13] A. Currao, V.R. Reddy, M.K. Veen, R.E.I. Schropp, G. Calzaferri, Photochem. Photobiol. Sci. 3 (2004) 1017.
[14] P. Wang, B.B. Huang, X.Y. Qin, X.Y. Zhang, Y. Dai, J.Y. Wei, M.-H. Whangbo, Angew. Chem. Int. Ed. 41 (2008) 7931.
[15] P. Wang, B.B. Huang, X.Y. Zhang, X.Y. Qin, H. Jin, Y. Dai, Z.Y. Wang, J.Y. Wei, J. Zhan, S.Y. Wang, J.P. Wang, M.-H. Whangbo, Chem. Eur. J. 15 (8) (2009) 1821.
[16] P. Wang, B.B. Huang, Q. Zhang, X.Y. Zhang, X.Y. Qin, Y. Dai, J. Zhan, J. Yu, H. Liu, Z. Lou, Chem. Eur. J. 16 (2010) 10042.
[17] H.M. Gong, X.H. Wang, Y.M. Du, Q.Q. Wang, J. Chem. Phys. 125 (2006) 024707.
[18] A. Kumar, V.J. Chaudhary, Photochem. Photobiol. A: Chem. 189 (2007) 272.
[19] A. Kumar, V.J. Chaudhary, Nanotechnol. 20 (2009) 095703.
[20] T. Priya, S.J. Satyawati, K. Sudhir, M. Tulsi, Langmuir 25 (11) (2009) 6377.
[21] K. Gill Simerjeet, J. Hope-Weeks Louisa, Chem. Commun. (2009) 4384.
[22] P.V. Kamat, Pure Appl. Chem. 74 (2002) 1693.
[23] T. Zywietz, J. Neugebauer, M. Scheffler, Appl. Phys. Lett. 73 (1998) 487.
[24] T. Zywietz, J. Neugebauer, M. Scheffler, J. Northrup, C.G.V. de Walle, MRS Internet J. Nitride Semicond. Res. 3 (1998) 26.
[25] J.P. Perdew, K. Burke, M. Ernzerhof, Phys. Rev. Lett. 77 (1996) 3865.
[26] P.E. Blöchl, Phys. Rev. B 50 (1994) 17953.
[27] G. Kresse, D. Joubert, Phys. Rev. B 59 (1999) 1758.
[28] G. Kresse, J. Hafner, Phys. Rev. B 47 (1993) 558.
[29] H.J. Monkhorst, J.D. Pack, Phys. Rev. B 16 (1977) 1748.
[30] L. Manna, L.W. Wang, R. Cingolani, A.P. Alivisatos, J. Phys. Chem. B 109 (2005) 6183.
[31] R. Di Felice, J.E. Northrup, Neugebauer, J. Phys. Rev. B 54 (1996) 17351.
[32] R. de Paiva, R. Di Felice, J. Phys. Chem. C 114 (9) (2010) 3998.
[33] J.H. Song, T. Akiyama, A.J. Freeman, Phys. Rev. B 77 (2008) 035332.
[34] B. Wen, R.V.N. Melnik, Appl. Phys. Lett. 92 (2008) 261911.
[35] J. Yang, J. Zeng, S. Yu, L. Yang, G. Zhou, Y. Qian, Chem. Mater. 12 (2000) 3259.
[36] K. Wright, J.D. Gale, Phys. Rev. B 70 (2004) 035211.
[37] J. Neugebauer, M. Cchеffler, Phys. Rev. B 46 (1992) 16067.
[38] R. Shaltaf1, E. Mete, S. Ellialtıoğlu, Phys. Rev. B 72 (2005) 205415.
[39] Y.D. Ma, H. Jin, Y. Dai, B.B. Huang, Appl. Surf. Sci. 256 (2010) 4136.
[40] J. Furthmüller, J. Hafner, G. Kresse, Phys. Rev. B 53 (1996) 7334.
[41] G. Kern, J. Hafner, G. Kresse, Surf. Sci. 366 (1996) 445.
[42] J. Robertson, M.J. Rutter, Diamond Relat. Mater 7 (1998) 620.
[43] W.X. Li, C. Stampfl, M. Scheffler, Phys. Rev. B 65 (2002) 075407.
[44] Z. Zeng, J.L.F. Da Silva, H. Deng, W. Li, Phys. Rev. B 79 (2009) 205413.
[45] J.C. Idrobo, S. Öğüt, J. Jellinek, Phys. Rev. B 72 (2005) 085445.
[46] S. Srinivas, U.A. Salian, J. Jellinek, in: N. Russo, D.R. Salahub (Eds.), Metal–Ligand Interactions in Biology, Chemistry, and Physics, Kluwer, Dordrecht, 2000, p. 295.